Probing the thermal resistance of solid-liquid interfaces in nanofluids with molecular dynamics

Article

Accepted Version

Probing the Thermal Resistance of Solid-Liquid Interfaces in Nanofluids with Molecular Dynamics

Iván Carrillo-Berdugo,[a,b,*] Javier Navas,[a] Ricardo Grau-Crespo[b]

[a] *Department of Physical Chemistry, Faculty of Sciences, University of Cadiz, 11510 Puerto Real, Cádiz, Spain.*

[b] *Department of Chemistry, University of Reading, Whiteknights, Reading, UK, RG6 6DX.*

* Corresponding author: **ivan.carrillo@uca.es** (I.C.-B.)

Abstract

The significance of the interfacial thermal resistance in the thermal conductivity of nanofluids is not well understood, in part because of the absence of measurements of this quantity in nanofluids of interest. Here we study the interfacial thermal resistance for metal-oil nanofluids of interest as heat-transfer fluids for concentrating solar power, using density functional theory and molecular dynamics simulations. Insights on the role of chemical interactions in the interfacial thermal resistance are revealed. The results presented here showcase a general picture in which the stronger the chemical interactions between species at interfaces, the lower the associated interfacial thermal resistance. The implications towards nanofluid design are discussed. We show that, for this important family of metal-oil nanofluids, the interfacial thermal resistance values are low enough so that it is possible to afford a reduction in particle size, minimising stability and rheology issues while still offering enhancement in the effective thermal conductivity with respect to the base fluid.

Keywords

nanofluids, interfacial thermal resistance, solid-liquid interface, thermal conductivity, density functional theory, molecular dynamics

I. Introduction

Nanofluids are colloidal suspensions of a nanostructured solid material (dispersed phase) in a fluid. They were first introduced nearly three decades ago[1] as promising heat-transfer fluids (HTFs), and since then, have been intensively studied for their potential in challenging heat transfer applications like concentrating solar power (CSP).[2,3] The International Energy Agency has highlighted the potential use of nanofluids as advanced heat transfer fluids in parabolic-trough collectors of CSP plants,[4] where nanofluids offer enhanced thermal conductivity and specific heat, compared to the conventional HTFs. The efficiency of the solar-to-thermal energy conversion in CSP plants is mostly determined by these properties of the energy-storing fluid as it flows through solar collectors and transfers heat through the thermodynamic cycle of the plant. A modest enhancement in these thermal properties using nanofluids can have significant consequences for the performance or design of CSP plants.[5]

There are abundant reports of substantial thermal conductivity enhancements in nanofluids, with respect to the base fluid, even at low volume fractions of nanomaterial.[6] Unfortunately, the overall picture of the thermal conductivity enhancements in nanofluids remains inconsistent, with wide variability between results reported by different authors, even for the same solid-liquid pair.[7,8] This lack of consistency of thermal conductivity enhancements, beyond modest gains, is one of the main causes of the current gap between expectation and reality in the use of nanofluids in heat transfer applications (another important factor contributing to that gap is that an increase in viscosity can detract from any thermal conductivity improvement in nanofluids[9]). Given that our work deals with the physico-chemical understanding of the effective thermal conductivity of nanofluids, we present below a short summary of existing controversies on the topic, and of the role of computer simulations in aiding that understanding.

The thermal conductivity of nanofluids has often been described as ‘anomalous’, a qualifier that underscores that measured values exceed those predicted by Maxwell’s effective medium

approach (EMA) model, which is suitable for composites of stationary, well-dispersed, non-interacting spherical particles with no interfacial thermal resistance (ITR) between them and the matrix. Keblinski *et al.*[10] have pointed out that the apparent disagreement between measured thermal conductivity values and EMA predictions for nanofluids is just a biased perception due to the limitations of Maxwell's model. In the same work, they verified that experimental data available at the time lay within the so-called Hashin-Shtrikman's bounds[11] for the thermal conductivity of suspensions, which are EMA-based. The lower bound describes suspensions of well-dispersed, non-interacting spherical particles (just like Maxwell's model), whereas the upper bound describes suspensions of clustered particles behaving as thermal resistances in parallel. The Hashin-Shtrikman's bounds, however, do not rationalise intermediate situations.

Keblinski *et al.*[12] defined the path for the search of phenomena explaining thermal conductivity enhancements beyond the Maxwell's limit in nanofluids. Many of the models that have been proposed in literature were developed under assumptions or boundary conditions that are contextualised in or motivated by the (non-mutually exclusive) phenomena explored in that work. They include, for instance, enhanced conduction through interphases due to liquid layering at solid-liquid interface, enhanced heat transfer due to translational Brownian motion of the particles, Brownian motion-induced convection in the liquid and, in the case of large volume fractions, preferential conduction through clusters of aggregated particles. Mugica and Poncet,[13] in a review of models built around the hypothesised phenomena, warned of their empiricism and lack of generality (in relation to most Brownian motion-based models, although the criticism is extensible to other models).

Almost a decade ago, Tertsinidou *et al.*,[7] motivated by discrepant datasets, inconclusive models, and conflicting statements in literature, presented a different appraisal of literature results. They came to the conclusion that, if established experimental methods are applied to the same thermodynamic systems, the observed thermal conductivity of nanofluids does align

with what one would anticipate from a simple conduction model in a stationary system with multiple phases. According to these authors, the existing variability responds to either a poor characterisation of the sample descriptors, or an incorrect use of the transient hot-wire technique (or functionally limited forms of the latter). Only a reduced collection of datasets was discriminated as reliable and those were found to agree with Maxwell's or Hamilton-Crosser's models, potentially refuting previous claims of 'anomalous' thermal conductivity in nanofluids. Antoniadis *et al.*[8] supported the discussion with results from thoroughly detailed measurements for a couple of case studies.

On the other hand, in a scientific debate with Assael and Wakeham,[14-16] Hasselman pointed out that the previously cited works of Tertsinidou *et al.* and Antoniadis *et al.* ignored possible compensating effect associated to the ITR of wire-fluid and particle-fluid interfaces and their temperature dependence. Therefore, the agreement of their data with Maxwell's or Hamilton-Crosser's models (which neglect the ITR values) could have been a fortuitous finding. Hasselman also speculates about the possibility of a strong temperature dependence of the ITR of particle-fluid interfaces being responsible for the positive temperature dependence of the thermal conductivity of nanofluids. He also advises to be cautious with the use of these models, as the ITR of particle-fluid interfaces has been proven to have a significant effect in some cases.[17] Assael and Wakeham counter-replied some of Hasselman's proposals but agreed on the fact the ITR of particle-fluid interfaces should be considered in order to rationalise the magnitude of the deviations of the thermal conductivity of nanofluids with respect to the upper limit defined by Maxwell's or Hamilton-Crosser's models, so we can have better predictions for assessing their engineering value.

Atomistic simulations, with realistic models founded on an *ab initio* basis, can play a central role in clarifying these issues, which has motivated computational studies of the thermal conductivity of nanofluids. Xue *et al.*[18, 19] used non-equilibrium molecular dynamics (NEMD)

simulations to generate temperature profiles in simple models that mimicked solid-liquid interfaces between a generic fcc-structured solid and a generic monoatomic liquid, whose interactions were described by Lennard-Jones potentials. By tuning the potential that describes solid-liquid interactions, they emulated two cases with qualitatively different wettability. They concluded that a wetting liquid exhibits clear stratification, but according to the temperature profiles thermal transport through the liquid at the interphase is indistinguishable from the bulk. They observed, however, that the temperature gap at the interface, to which the ITR is directly proportional, is significantly reduced as wettability increases. Eapen *et al.*[20, 21] followed a similar working scheme for NEMD simulations with simple models of solid clusters uniformly dispersed in a monoatomic liquid, whose interactions were also described by Lennard-Jones potentials. They verified that the stronger the interactions between species at solid-liquid interfaces, the lower the ITR and the closer the thermal conductivity value to the upper Hashin-Shtrikman's bound, and *vice versa*. These works and those of others,[22-27] although many of them are not strictly related to actual materials, provided useful directions to continue investigating the significance of interactions between species at solid-liquid interfaces for the ITR.

Here, we study the ITR of solid-liquid interfaces of specific materials of interest for heat transfer nanofluids with application in CSP, using a combination of density functional theory (DFT) and NEMD simulations. The liquid of interest is the eutectic and azeotropic mixture of 73.5% diphenyl ether (DPO) and 26.5% biphenyl (BP), commercially available as a HTF for CSP plants with parabolic-trough collectors under the name of Dowtherm A or Therminol VP-1. The solids of interest will be metals, the second-most studied group of materials for nanofluids, just after metal oxides, due to their very high thermal conductivity. We consider Ni, Cu, Pd, Ag, Pt and Au, group 10 and 11 transition metals with a varied surface chemistry for interactions with the phenyl rings in the molecular liquid. The work is structured into three

sections: (i) study of the adsorption of DPO and BP on transition metal surfaces at the DFT level-of-theory, (ii) replication of adsorption behaviour at the MD level-of-theory, and (iii) estimation of ITR values using NEMD simulations. The ITR values will inform the discussion on whether the negative effect of a thermal resistance is significant or not, considering the particle sizes that are typically available for metal nanoparticles manufactured in powder form.

II. Methodology

A. DFT simulations

We used the Vienna Ab initio Simulation Package (VASP)[28-31] for first-principles simulations at the periodic-DFT level. For the study of adsorption geometries and energies we considered models with (111)- and (100)-terminated slabs of each metal, of thickness equal to four atomic layers, and limited by a vacuum slab of 20.0 Å that minimises unphysical interactions between periodic images along the surface normal direction. Molecules were initially allocated on the surface so that each phenyl ring is placed onto one of the high-symmetry sites described in **Figure 1**. Slab models were submitted for full relaxation of the ionic positions. For the study of adsorption kinetics, we used the nudged elastic-band (NEB) method,[32, 33] which approximates the minimum-energy pathway (MEP) for adsorption by performing a constrained optimisation of five linearly interpolated images between the gas phase molecular geometry and the most stable adsorbed molecular geometry for each molecule on each surface, aiming for the minimisation of the forces acting on each image. In all these calculations, the Perdew-Burke-Ernzernhof (PBE) functional,[34, 35] based on the generalised gradient approximation (GGA), was used to describe the exchange-correlation energy term in the resolution of Kohn-Sham equations. The Grimme's dispersion correction method (D3)[36] with the Becke-Johnson damping function[37] was included to describe van der Waals interactions. The GGA-PBE functional with D3 corrections has been proven to work well for the adsorption of aromatic

species on metal surfaces, with some overestimation in their adsorption energy.[38] Valence wavefunctions were described by sets of planewaves with kinetic energies up to 400 eV (extended up to 520 eV for the optimisation of the unit cell lattice parameters of each metal). Interactions between valence electrons and ionic cores were described using the projector-augmented wave (PAW) pseudopotentials,[39, 40] where electron states up to 1s in C and O, up to 3p for Ni and Cu, up to 4p for Pd and Ag and up to 4f for Pt and Au were frozen to atomic reference states. Brillouin-zone integrations were performed using 3×3×1 k-point grids generated by the Monkhorst-Pack method[41, 42] (the required density of k-points in reciprocal space was determined from convergence tests in the bulk metals). The Methfessel-Paxton smearing method,[43] with an electronic temperature of 0.2 eV, was used to describe orbital occupancies during calculations. Spin-polarised calculations were performed in slabs containing Ni, which is ferromagnetic. Dipole moment corrections to the total energy were applied in slab calculations. Visualisations of models for DFT simulations were made with OVITO.[44]

B. Morse potential parametrisation

Morse potential parameters for carbon-metal interactions in MD simulations were derived using the fitting feature available in the General Utility Lattice Program (GULP).[45-49] GULP takes a reference dataset of structures and energies and uses the Newton-Raphson approach for fitting the potential parameters by minimisation of the weighted sum of squares of the difference between the reference energy and that estimated by the potential for each structure. Reference datasets were constructed from *ab initio* PESs, scanned by running single-point energy calculations at the DFT level in VASP (using the exact same setup described in the previous section) over a series of structures with regular shifts in the perpendicular distance of the adsorbed molecule to the surface with respect to the minimum energy structure. A dataset was

generated for each relevant geometry in **Figure 2**, and the resulting sets of potential parameters were grouped and averaged by metal surface and presented in **Table 2**.

C. MD simulations

We used the Large Atomic/Molecular Massively Parallel Simulator (LAMMPS)[50-52] for classical MD simulations and the Moltemplate[53, 54] text-based builder for atomistic modelling. For the study of the ITR, we considered models with (111)-terminated metal slabs, with 77,280 metal atoms distributed into thirty atomic layers, in direct contact with a liquid slab composed of a mixture of DPO and BP molecules, with a total of 3,456 randomly distributed molecules in the same proportion as in the actual HTF. These models contain a sufficiently large number of particles to fulfil the thermodynamic limit condition. Interactions between atom species in the metal slab were described with the MEAM potential, with parameters generated by the MEAM Parameter Calibration tool.[55] The energy-volume curve and the (111) and (100) surface energies from DFT calculations were used as calibration targets. Interactions between atom species in the liquid slab were described with the OPLS-AA force field, with parameters by Jorgensen *et al.*[56-58] Lennard-Jones pairwise interactions and Coulomb electrostatics between atom species in the liquid matrix were limited to a cut-off distance of 10.0 Å. Long-range electrostatics were approximated by the particle-particle particle-mesh (PPPM) summation method.[59] The MEAM potential and the OPLS-AA force field were validated for the calculation of different thermodynamic properties of the metals and the organic molecular liquid. Data for validation is available at **Figures S1** and **S2** of the Supplementary Material. Interactions between species at the interface were described with the Morse potentials parametrised in this work, limited to a cut-off distance of 8.0 Å. Periodic boundary conditions were set for all models. All models' dimensions are sufficiently large (above 110 Å in all directions after equilibration) to ensure that the largest cut-off distance is less than half the simulation box length in any direction, thus meeting the minimum-image convention, and less than half the

thickness of the solid and liquid slabs, so that no confinement effects are expected. The Verlet integration scheme[60] was used. Thermostatting and barostatting were performed by the Nosé-Hoover schemes.[61-64] A typical MD simulation for these systems comprises of an equilibration run for 2.0 ns under NPT conditions with a time step of 1.0 fs, and a production run for 2.0 ns under NVE conditions with a time step of 0.25 fs. The production run is a NEMD run in which a temperature gradient is induced in the model, along the direction perpendicular to the solid-liquid interface (the *z*-direction of the simulation cell) as a response to an imposed heat flux. This working scheme is known as the Müller-Plathe scheme.[65] The simulation cell is divided into $N = 50$ bins along the *z*-direction. Bin 1 and bin $N/2 + 1$ correspond to the heat sink and the heat source, respectively. The heat flux results of exchanging velocities between the coldest atom in the heat source and the hottest atom in the heat sink. As the atoms have different masses, the exchange is relative to their centre of mass, so that energy and linear momentum are conserved. Velocity exchanges are performed once every 100 steps. The total heat is the sum of kinetic energy transferred in velocity exchanges over the run time. The temperature gradient develops along the *z*-direction and the profile plot is built from bin local temperatures, which are well-converged averages over the number of particles in each bin and the run time after a steady-state heat flux is reached. All Moltemplate and LAMMPS input files, including force field parameters, structures and run setup are available in the Supplementary Material. Visualisations of models for MD simulations were also made with OVITO.[44]

III. Results and Discussion

A. Adsorption of DPO and BP on transition metal surfaces

We first focus on the adsorption of DPO and BP molecules on (111) and (100) surfaces of Ni, Pd, Pt, Cu, Ag and Au, which is studied *via* first-principles DFT simulations within VASP.[28-31] DFT is expected to provide the necessary thermodynamic and kinetic parameters about the

adsorption process to reliably model metal-organic liquid interfaces for MD simulations, in which the ITR is calculated.

The adsorption of benzene on transition metals has been profusely studied before using DFT.[38, 66-73] Morin *et al.*[66] provided an exhaustive electronic analysis, also at the DFT level of theory, for the adsorption of benzene on some group 9 and 10 transition metal surfaces. They determined that adsorption is mediated by donation of electrons from the highest occupied π molecular orbital of the aromatic species to the d_{z^2}-band of the metal and back-donation from the d_{z^2}-band to the lowest unoccupied π* molecular orbital. The donation and back-donation of electrons requires p_z orbitals of C atoms (contributing to π and π* molecular orbitals) and d_{z^2} orbitals of metal atoms at the surface (contributing to the d_{z^2}-band) to overlap. Therefore, adsorption of phenyl rings only occurs when these structures lying flat on these sites of the metal surface whose symmetry allows the alignment of these orbitals. The notation[74] to label these high-symmetry sites of (111) and (100) fcc metal surfaces refers to the relative position of the geometric centre of the aromatic ring with respect to the surface: Bri, ^{hcp}H, ^{fcc}H, ^{4f}H and Atop stand for bridging, hcp-packed hollow, fcc-packed hollow, 4-fold hollow, and atop of an atom sites, respectively. The 3-fold symmetry of the (111) surface allows the ring to adsorb with different orientations, 0º or 30º, depending on the degree of rotation of the aromatic ring with respect to the surface lattice vectors. **Figure 1** shows the schematics of these sites for each surface.

For the study of the adsorption of DPO and BP on (111) and (100) metal surfaces, we considered initial geometries in which the phenyl groups of these molecules are simultaneously allocated on two of these sites. This totals to 78 possible initial geometries for each metal, but the constraints imposed by the link between phenyl groups reduces this number to 36. After full ionic relaxation at the DFT level-of-theory, only 9 stable non-redundant geometries were found for each metal. We checked that these adsorption geometries correspond to minima in the

corresponding potential energy surfaces, by confirming real frequencies of vibration of the molecules (see Supplementary Material). None of them corresponds to a dissociative adsorption process. **Table 1** identifies which sites on the (111) and (100) metal surfaces are occupied upon adsorption of DPO and BP molecules with the relevant geometries and lists the adsorption energy for each case, calculated as the difference between the energy of the relaxed adsorbate-adsorbent slab, and the sum of the energies of the relaxed metal surface slab and the relaxed molecule isolated in gas phase.

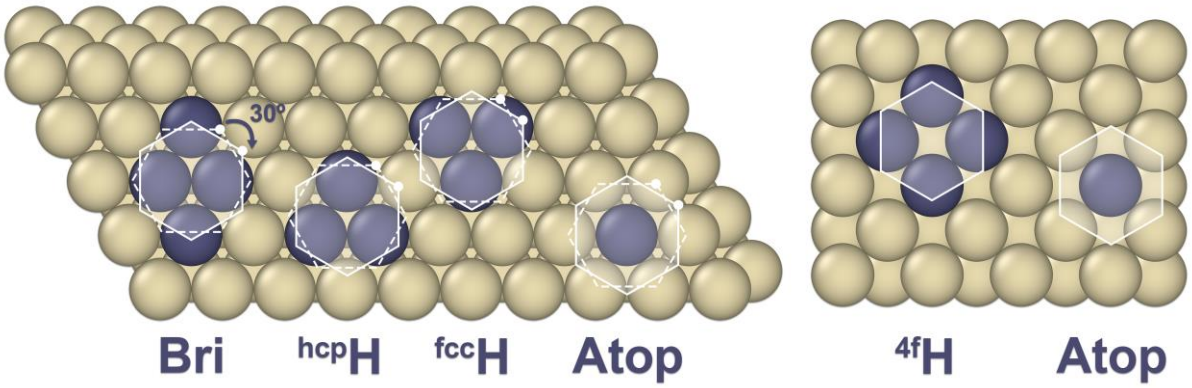

Figure 1. Adsorption sites on the (111) surface (left) and the (100) surface (right) of fcc-structured transition metals.

Table 1 shows that for any given molecule or termination, the adsorption energy is much higher on Ni, Pd and Pt (group 10 elements) surfaces than on Cu, Ag and Au (group 11 elements) surfaces. This finding agrees with the general observation of similar chemistry for elements in each group of the periodic system because they have homologous valence electronic configurations. Within the context of the donation and back-donation mechanism presented by Morin *et al.*,[66] which holds for the adsorption of phenyl groups of DPO and BP molecules as well, the relative differences in the filling of the d_{z^2}-band between elemental metals of groups 10 and 11 can explain why adsorption energy is higher on Ni, Pd and Pt surfaces (10 valence electrons per atom) than on Cu, Ag and Au surfaces (11 valence electrons per atom). While the

adsorption of aromatics on group 10 metal surfaces is known to be due to covalent bonding and van der Waals interactions (*i.e.*, chemisorption), on group 11 metal surfaces is almost completely due to van der Waals interactions (*i.e.*, physisorption).[70]

Table 1. Adsorption energies, E_{ads}, for DPO and BP molecules on (111) and (100) surface terminations of group 10 and group 11 transition metals. Lowest energy geometries are highlighted in bold.

Surface	**Molecule**	**Adsorption sites**		**E_{ads} / eV**					
				Ni	Pd	Pt	Cu	Ag	Au
(111)	DPO	Bri_{30^o}	Bri_{30^o}	**-3.48**	**-3.93**	**-3.77**	**-1.63**	-1.34	-1.47
		Bri_{30^o}	$^{hcp}H_{0^o}$	-3.40	-3.82	-3.45	-1.63	-1.34	**-1.49**
		Bri_{30^o}	$^{fcc}H_{0^o}$	-3.39	-3.78	-2.96	-1.63	**-1.35**	-1.48
		$^{hcp}H_{0^o}$	$^{hcp}H_{0^o}$	-3.38	-3.62	-2.88	-1.62	-1.31	-1.46
		$^{fcc}H_{0^o}$	$^{fcc}H_{0^o}$	-2.83	-3.53	-2.89	-1.61	-1.34	-1.45
	BP	Bri_{30^o}	Bri_{30^o}	**-3.83**	**-4.07**	**-3.69**	**-1.85**	**-1.48**	-1.59
		$^{hcp}H_{0^o}$	$^{fcc}H_{0^o}$	-3.45	-3.65	-3.04	-1.90	-1.48	**-1.60**
(100)	DPO	^{4f}H	^{4f}H	**-4.68**	**-4.68**	**-5.70**	**-1.85**	**-1.37**	**-1.55**
	BP	^{4f}H	^{4f}H	**-4.55**	**-4.62**	**-5.36**	**-2.10**	**-1.52**	**-1.67**

Figure 2 visualises the minimum energy (most stable) geometries for absorbed DPO and BP on (111) and (100) surface terminations of group 10 and 11 transition metals. Phenyl rings lie parallel to the surface in all cases, but much closer and with better symmetry alignment on group 10 metals due to chemical bonding. In this case, C–H bonds bend out-of-plane, which is a characteristic structural distortion arising from steric effects forced by chemisorption.[75]

Figure 2 and **Table 1** also showcase that Bri_{30^o}, $^{hcp}H_{0^o}$ and $^{fcc}H_{0^o}$ sites on (111) surfaces and the ^{4f}H site on (100) surfaces are the only sites participating in the most stable adsorption geometries of DPO and BP. Adsorption on Ni, Pd and Pt (111) surfaces preferentially occurs on Bri_{30^o} sites over $^{hcp}H_{0^o}$ and $^{fcc}H_{0^o}$ sites, because phenyl groups on Bri_{30^o} sites are simultaneously coordinated to four metal atoms, whilst those on $^{hcp}H_{0^o}$ and $^{fcc}H_{0^o}$ are coordinated to only three. Such differences are not present or as significant on Cu, Ag and Au (111) surfaces.

This further proves that group 11 metals are not susceptible to donation and back-donation of electrons and that adsorption on their surfaces is predominantly determined by van der Waals interactions.

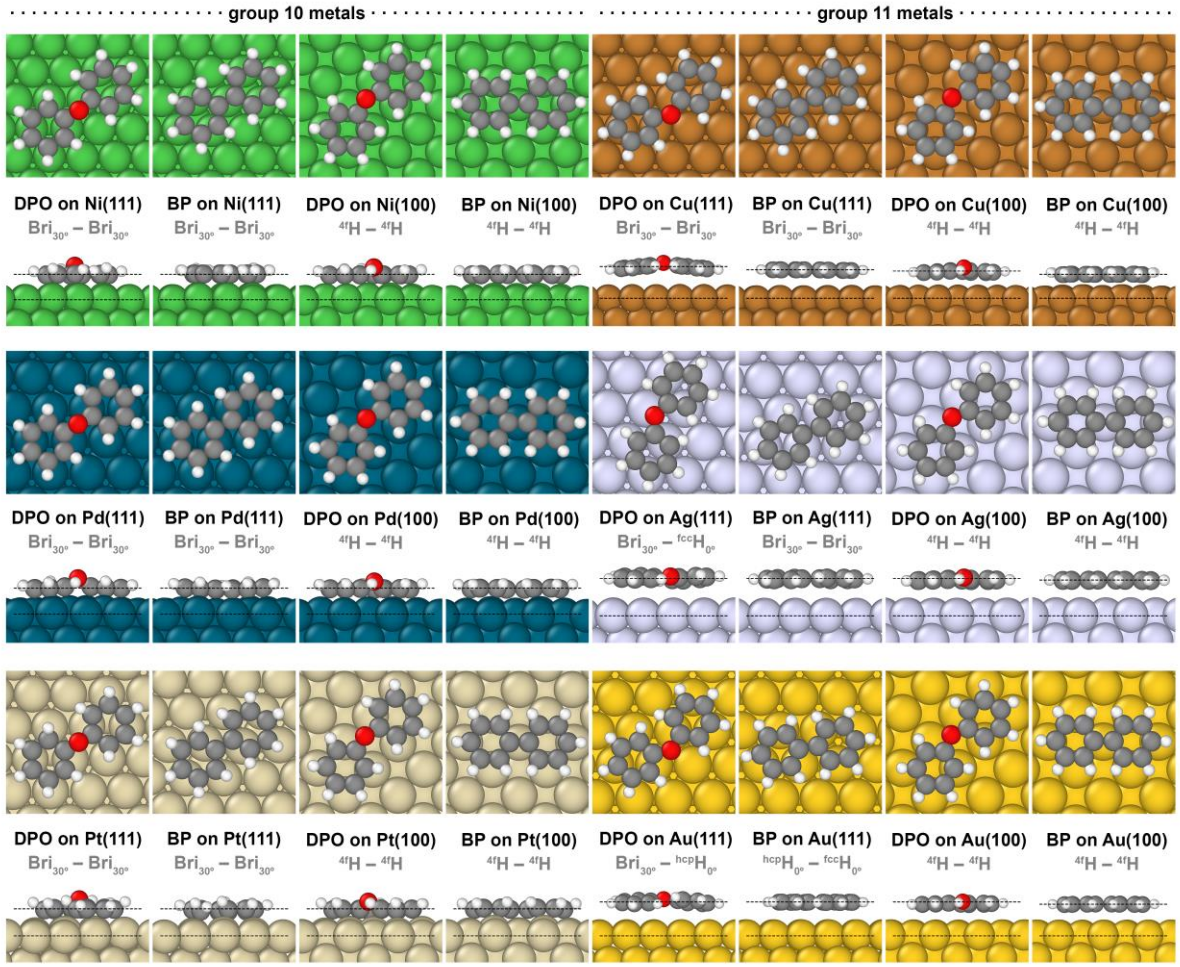

Figure 2. Top and front view of the minimum energy molecular geometries for adsorbed diphenyl oxide and biphenyl on (111) and (100) surface terminations of group 10 and 11 transition metals.

To understand the kinetics of the adsorption process, we have also calculated the activation energy of the MEP for the adsorption of the molecules, from gas phase, onto the target sites at the surfaces. MEPs are approximated using the NEB method,[32,33] which performs a constrained optimisation of images along a linearly interpolated pathway between the gas phase molecular geometry and the most stable adsorbed molecular geometry, aiming for the minimisation of the

forces acting on each image. **Figure 3** shows the MEP for the adsorption of each molecule on each surface, as a function of the perpendicular distance, *d*, between them (calculated as the distance between the mean plane defined by C atoms in phenyl groups and the mean plane defined by metal atoms at the surface). No significant saddle points were found along any of the MEPs, which means no kinetic barriers exist and no activation energy is required for either DPO or BP to adsorb on any of the surfaces under study.

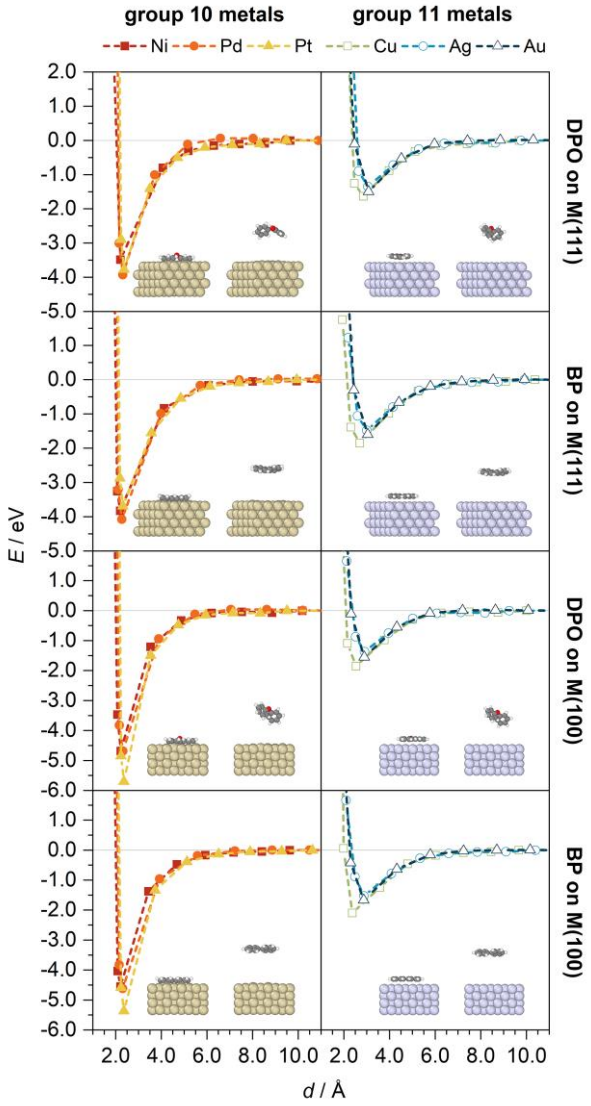

Figure 3. Minimum energy paths for the adsorption of diphenyl oxide and biphenyl molecules on (111) and (100) surface terminations of group 10 and 11 transition metals.

The outcome of first principles DFT calculations provides useful insights on how to model the metal-organic liquid interfaces with classical MD simulations. The adsorption energies indicate that the attachment of DPO and BP molecules to the surfaces is thermodynamically favoured on all transition metal surfaces under study. When the fluid composed of these molecules is in contact with a metal surface of one of these elements, the formation of a layer of adsorbed DPO and BP molecules should be expected at the interface between them. Given the absence of kinetic barriers, and the fact that adsorption energies are similar for both molecules at a given metal surface, we can assume that the molecular layer is formed as a random deposition from the fluid and therefore the composition of such adsorbed layer can be expected be the roughly same as that of the bulk fluid. Considering that adsorption energies per molecule are around 1.5 eV on Cu, Ag and Au surfaces and around 4.0 eV on Ni, Pd and Pt surfaces, that the liquid bulk cohesive energy is around -0.77 eV per molecule, and that the energy of thermal vibrations are in the order of $k_B T$ (*i.e.*, *ca.* 58 meV at 673 K), such layer of adsorbed molecules should be expected to remain stable even at the highest operation temperature for the bulk fluid. Therefore, whatever the effect of this layer of adsorbed molecules is on the ITR, such effect should still be observable at elevated temperatures. In the following sections of this work, we aim to evaluate that effect numerically, considering the subtleties arising from the unique chemistry of surfaces constituted by transitions metals in group 10 and 11 of the periodic system.

B. From DFT to MD: *ab-initio* parametrisation of classical potentials

Classical MD simulations constitute a convenient tool for the analysis of macroscopic properties, estimated as ensemble averages of a representative statistical ensemble generated by running a sufficiently long trajectory of an atomistic model of the system of interest, under either equilibrium or non-equilibrium conditions. A trajectory is the result of the numerical integration of the equations of motion for all atoms in the model, whose interactions are

governed by a classical force field. The quality of MD estimates relies on how accurately these interactions are described by the force field.

There are well established force fields for the calculation of structural and thermodynamic indicators of most homogeneous systems, as is the case of the Modified Embedded Atom Model (MEAM) for metals or the Optimised Potential for Liquid Simulations (OPLS) for organic molecular liquids, which we use in our MD simulations in this work. Force fields provide parameters for different atom types which can often be combined (under certain rules) to describe the interactions between atom types. However, combination rules tend to be unsatisfactory when used for the description of interactions between species at the interface between different chemical environments in heterogeneous systems.[76] Our work is sensitive to this issue, as we intend to calculate the ITR between a metal solid phase and an organic molecular liquid phase. For a correct description of the interface in each case, we need an interatomic potential that is correctly parametrised to account for the adsorption of phenyl groups on different metal surfaces. Here we have used the Morse potential, given by

$$U(r_{ij}) = D_0 \left[e^{-2\,\alpha\,(r_{ij}-r_0)} - 2\,e^{-\alpha\,(r_{ij}-r_0)} \right] \quad (1)$$

where r_0 is the equilibrium distance between the interacting atoms, and D_0 and α are the depth and curvature of the potential energy well, respectively. The tail of the Morse potential correctly describes the anharmonicity of bonding interactions and fairly approximates (although it is not fundamentally intended to) the attractive contribution of van der Waals interactions (for any $r_{ij} < r_{cutoff}$), which justifies its choice for the description of molecular adsorption in MD simulations of this work and precedent ones in literature.[77-79]

First-principles DFT calculations, as we saw in the previous section, provide a consistent picture of the adsorption trends of DPO and BP on surfaces of different transition metals across the periodic table. This encouraged us to use DFT to explore the potential energy surface (PES) of the adsorbate-adsorbent interaction of all relevant cases and generate reference datasets of

structures and energies for fitting Morse potentials for carbon-metal interactions using the fitting feature available in GULP.[45-49] The sets of fitted parameters are available in **Table 2**. No potentials have been parametrised for hydrogen-metal and oxygen-metal dispersive interactions in this work, as they are expected to be small contributors to the relevant PESs, particularly in those cases in which chemical bonding is involved.

Table 2. *Ab initio* derived Morse potential parameters for the representation of carbon-metal interactions in classical molecular dynamics simulations of the metal-molecular liquid interfaces.

Interaction	D_0 / eV	α / Å^{-1}	r_0 / Å
C – Ni(111)	0.1714	3.014	2.108
C – Ni(100)	0.2084	2.686	2.123
C – Pd(111)	0.2032	2.769	2.251
C – Pd(100)	0.2464	2.538	2.256
C – Pt(111)	0.2121	3.462	2.187
C – Pt(100)	0.3233	2.959	2.188
C – Cu(111)	0.0150	1.220	3.416
C – Cu(100)	0.0369	1.679	2.789
C – Ag(111)	0.0173	1.291	3.624
C – Ag(100)	0.0195	1.355	3.557
C – Au(111)	0.0192	1.213	3.709
C – Au(100)	0.0228	1.110	3.660

Figure 4 shows that the parametrised Morse potentials estimate PESs (line plots) that match the *ab initio* scanned PESs (scatter plots) with excellent agreement, reproducing fine details such as the perpendicular distance of the adsorbed molecule to the surface or its adsorption energy with sufficient accuracy. These potentials can effectively discriminate the physisorption of phenyl groups on surfaces of group 11 transition metals from the chemisorption on those of group 10 transition metals. The latter is characterised by deeper, narrower potential wells (higher values of D_0 and α). An important observation at this point is that such accuracy is met

using a unique set of parameters for the carbon-metal interaction on each surface. This does not constitute a problem unless the simulation involves migration of molecules between surfaces, which is not the case in our study. In fact, we expect that the set of parameters obtained is transferable for phenyl groups in either DPO or BP molecules (and, likely, in other molecules of similar structure) on a given transition metal surface.

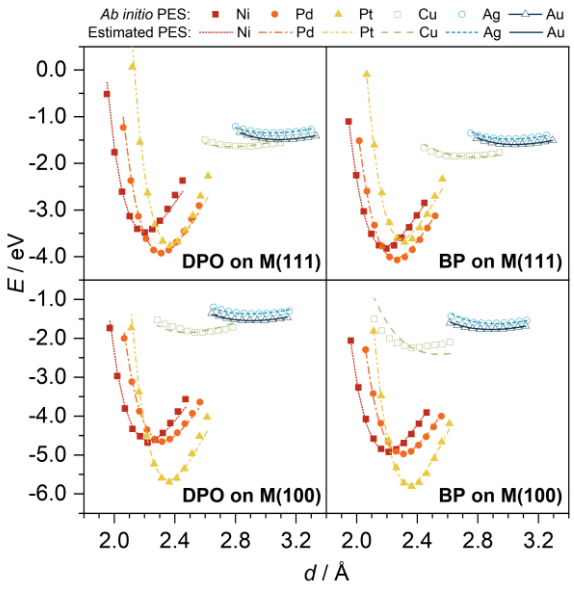

Figure 4. Comparison of the *ab initio* scanned and estimated potential energy surfaces for the interaction of diphenyl oxide and biphenyl with the (111) and (100) surface terminations of group 10 and 11 transition metals.

C. Interfacial thermal resistance of metal-molecular liquid interfaces and its implications

The ITR, also referred to as the Kapitza resistance, R_K, represents a measure of the obstruction to heat conduction between two dissimilar phases. The ITR is directly proportional to the temperature gap, ΔT, that disrupts the temperature gradient developed under a steady-state heat flux, J, applied across the interface between them:

$$R_K = \Delta T\, J^{-1} \tag{5}$$

We now describe our calculation of R_K values for the metal-molecular liquid interfaces of interest by exploiting its macroscopic definition in MD simulations with LAMMPS.[50-52] A

schematic view of the atomistic models for the metal-molecular liquid interfaces of interest is illustrated in **Figure 5**. In each model we consider a (111)-terminated metal slab, composed of a single metal type, in contact with a liquid slab, composed of a mixture of DPO and BP molecules in the same proportion as in the actual HTF. The choice of the (111)-termination for our MD models responds to the fact that most common nanoparticle shapes of fcc metals are completely or predominantly encased by this crystallographic facet.[80] Interactions between atom species in the metal slab were described with the MEAM potentials, and those in the liquid slab were described with the OPLS-AA force field. Interactions between species at the interface were described with the Morse potentials parametrised as described in the previous section of this work. Each model is equilibrated at either $T = 298$ K or 523 K and $P = 1.013$ bar, to investigate the effect of temperature on the ITR.

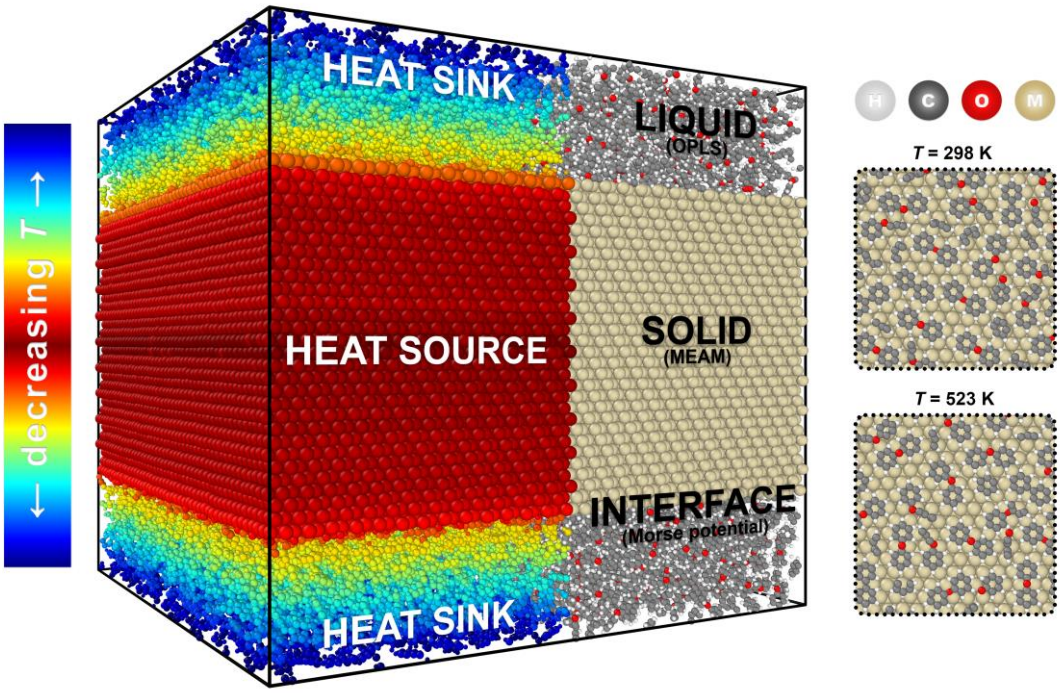

Figure 5. Schematic view of the atomistic models for metal-molecular liquid interfaces. The plan views show the actual structure of the solid-liquid interface after equilibration, consisting mostly of flat-lying molecules on a Pt(111) surface termination. Colour gradient shows the temperature profile induced along the direction perpendicular to the interface using the Müller-Plathe method.

The plan views in **Figure 5** depict that high surface coverage and mostly planar adsorption are achieved even under high temperature conditions, resulting in metal surfaces permanently decorated by a molecular patchwork. This proves that we can rely on the parametrised Morse potentials for the replication of the adsorption of aromatic species on transition metal surfaces in MD simulations, as it mimics, with excellent agreement, the geometries from DFT simulations.

We proceeded as indicated by the Müller-Plathe reverse NEMD scheme,[65] which is already implemented in stable releases of LAMMPS, to induce a temperature gradient along the direction perpendicular to the interface (the *z*-direction of the simulation cell) by imposing a heat flux generated by exchanging the velocities of atoms contained in the regions defined as heat source and heat sink in **Figure 5**. The NEMD-generated temperature profiles are shown in **Figure 6 (a)**, overlayed on a cross-sectional view of the atomistic models of solid-liquid interfaces between the liquid mixture of DPO and BP and the (111) surface terminations of Pt and Ag (as examples of group 10 and 11 transition metals, respectively). The temperature gaps that discontinue the profiles appear, as expected, at the solid-liquid interfaces, and the ΔT gaps are noticeably different for interfaces with surface terminations of metals from each group.

The R_K values are plotted in **Figure 6 (b)** *vs.* the stiffness, *S*, of the metal-carbon interactions at the interface. *S* is an unbiased quantifier of the strength of such interactions. For the Morse potential, which is the one that represents the chemical interactions between species at the interfaces in our models, *S* is the harmonic expansion coefficient that appears by expanding the potential $U(r_{ij})$, as written in expression (1), as a Taylor series around $r_{ij} = r_0$:

$$S = 2\, D_0\, \alpha^2 \qquad (2)$$

where D_0 and α are the depth and curvature of the potential energy well that characterises the interaction, which are previously reported in **Table 2**. The R_K *vs. S* plot provides a convenient picture for the discussion of the ITR in terms of the chemistry of the interfaces. Cross-model comparison is reliable as long as no sources of bias are identified. Here, all the models involve

the same liquid phase and the same surface termination for the solid phase and differ only in the nature and interface chemistry of the constituent metal of the solid phase, which is represented in our models by using the *ab initio* parametrised MEAM and Morse potentials. Besides, the parametrisations of the potentials that describe the interactions between atom species in the liquid phase, the solid phase and the interface are well constrained to the same level-of-theory within the relevant region.

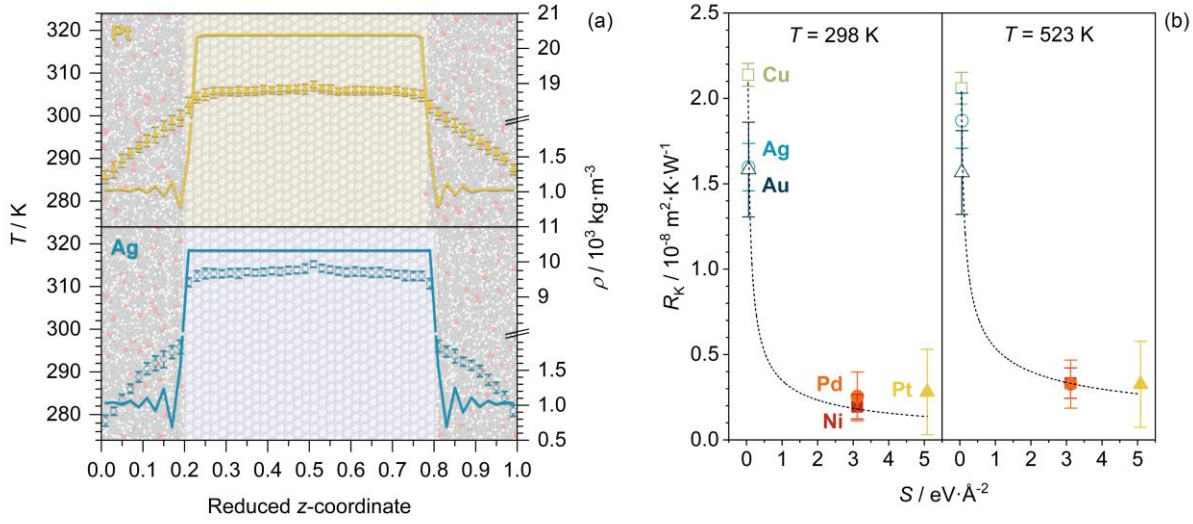

Figure 6. (a) Temperature (scatter) and density (solid line) profiles of the atomistic models of metal-molecular liquid interfaces with Pt and Ag, at average $T = 298$ K. (b) Relationship between the thermal resistance (calculated at either $T = 298$ K or $T = 523$ K) and the stiffness of the metal-carbon interaction at the interface.

The main conclusion that stems from **Figure 6 (b)**, in view of the power-law decreasing R_K values with increasing S values, is that strong chemical interactions between solids and liquids result in interfaces of low thermal resistance. The difference in R_K values can be as significant as one order of magnitude when comparing the interfaces with group 10 and group 11 transition metals, on which the liquid phase molecules, due to the unique surface chemistry of each group of metals, can chemisorb (high S values, > 3.0 eV·Å^{-2}) and physisorb (low S values, < 0.1 eV·Å^{-2}), respectively. The effect of temperature on the ITR, however, is practically

negligible. This finding is consistent with our previous observation on the preservation of the composition, distribution, and adsorption geometry of molecules at these metal surfaces within the range of temperatures studied here (see **Figure 5**). The temperature independence of R_K values here reported seem to refute the hypothesis of Hasselman[14] on the positive temperature dependence of the thermal conductivity of nanofluids due to a negative temperature dependence of the ITR of particle-fluid interfaces.

There is, unfortunately, no experimental or theoretical data available for the thermal resistance of this unique set of interfaces, but we can contextualise our work by comparing the computed R_K values to those of other interfaces. For instance, Alosious *et al.*[81, 82] have previously studied the ITR of carbon-water interfaces in aqueous systems with graphene and carbon nanotubes using NEMD. They reported R_K values of *ca.* $3.0 \cdot 10^{-8}$ $m^{-2} \cdot K \cdot W^{-1}$. No chemical interactions beyond van der Waals forces are expected in these interfaces, in which C – O interactions were modelled by a Lennard-Jones potential with $\varepsilon = 4.063 \cdot 10^{-3}$ eV and $\sigma = 3.190$ Å. By expanding the Lennard-Jones potential as a Taylor series around $r_{ij} = r_0$, as we did for the Morse potential, we can estimate S values for C – O interactions of *ca.* 0.03 $eV \cdot Å^{-2}$. The interactions in carbon-water interfaces are much weaker compared to our metal-oil interfaces, and their ITR is also notably higher, which further supports the general picture illustrated in our work: the stronger the interactions between species at solid-liquid interfaces, the lower the ITR, and *vice versa*.

Another finding to point out from NEMD calculations are the density anomalies in the liquid phase in the vicinity of the interface, as shown in **Figure 6 (a)**. These are indicative of liquid layering, a gradual stratification of the liquid with denser layers towards the solid surface termination, resulting in an inhomogeneous space region between the two phases in contact that is referred as interphase. This phenomenon is reproduced in our models by the long-range influence of the Morse potential, whose anharmonic tail approximates van der Waals

interactions. Liquid layering has been previously postulated in literature[18, 19, 83, 84] to be partially responsible for the thermal conductivity enhancements in nanofluids, due to largely ordered liquid structures of purportedly higher thermal conductivity at the interphase, compared to the liquid bulk. However, as the temperature gradient of the liquid is practically linear over the entire cross-section, the natural conclusion is that the thermal conductivity of the liquid at the interphase is no different, or at least not significantly different, from that at the bulk. Therefore, liquid layering seems to be irrelevant for thermal conductivity enhancements in these nanofluids, although it can have a positive effect for specific heat enhancements, as reported by our group for the case of Pd.[85, 86] In other systems, such as fluid flow through nanochannels, the severe miniaturisation of the conduit results into confinement of the fluid between two surfaces, in which case the transport properties of the confined fluid can be significantly different to those of the bulk, as reported by Liakopoulos *et al.*[87, 88]

We now return to the question that motivates this work: is the negative effect of the thermal resistance significant, considering the particle sizes that are typically available for metal nanoparticles manufactured in powder form? A qualitative answer to this question can be provided by discussing the trends captured by the Biot number, Bi, which is a non-dimensional combination of the particle diameter, d, the interfacial thermal resistance, R_K, and the thermal conductivity of the liquid, κ_L:

$$Bi = \frac{d}{2\, R_K\, \kappa_L} \tag{3}$$

Bi quantifies the impact of R_K on the overall heat conduction process. Bi^{-1} appears, for instance, in extended versions of Maxwell's EMA-based model for the effective thermal conductivity, κ_{eff}, of particulate composites (nanofluids can be classified as such), including the interfacial thermal resistance. We refer to the works of Hasselmann and Johnson[89] and Nan *et al.*[90] for some simple yet compelling limiting cases of interest. For instance, the formulation of

κ_{eff} for composites with a variable volume fraction, ϕ, of spherical particles with thermal conductivity κ_S:

$$\frac{\kappa_{\mathrm{eff}}}{\kappa_{\mathrm{L}}} = \frac{\kappa_{\mathrm{S}}\,(1 + 2\,Bi^{-1}) + 2\,\kappa_{\mathrm{L}} + 2\,\phi\,[\kappa_{\mathrm{S}}\,(1 - Bi^{-1}) - \kappa_{\mathrm{L}}]}{\kappa_{\mathrm{S}}\,(1 + 2\,Bi^{-1}) + 2\,\kappa_{\mathrm{L}} - \phi\,[\kappa_{\mathrm{S}}\,(1 - Bi^{-1}) - \kappa_{\mathrm{L}}]} \qquad (4)$$

If $R_K = 0$ is assumed, then $Bi^{-1} = 0$ and expression (4) results into the original expression of Maxwell for κ_{eff}, so that $\kappa_{eff}/\kappa_L > 1$ for any $\phi > 0$ if $\kappa_S > \kappa_L$. In reality, $R_K > 0$, so $\kappa_{eff}/\kappa_L > 1$ can only be achieved if an additional condition is fulfilled: we are operating with sufficiently large particle sizes, d, so that $Bi^{-1}(d) < 1$.

Figure 7 shows the plot of Bi^{-1} *vs.* d, as the particle size is the only feature affecting this dimensionless quantity that is not intrinsic to the relevant materials we have studied here and can be independently controlled. In the arithmetic behind it we included the κ_L and R_K values computed in this work. All plots are referred to the same liquid, therefore any changes to be discussed are due to the R_K values of the different interfaces. The Bi^{-1} *vs.* d curves convey that the effect of R_K vanishes even for small d values. Heat conduction across the solid-liquid interface can objectively be considered non-restrictive (*i.e.*, $Bi^{-1} < 1$) for particle sizes over *ca.* 1 nm for group 10 metals and *ca.* 2-5 nm for group 11 metals, depending on the R_K values of their interfaces. This answers the previously introduced question: from a practical point of view, this condition can be expected to be easily met for most commercially available metal nanoparticles, with particle sizes typically ranging within 40-80 nm, but there is room for particle size reduction with synthetic approaches so that Bi^{-1} remains small enough for the ITR not to limit the effective thermal conductivity. Rheology and stability issues are also less likely with smaller particle sizes.

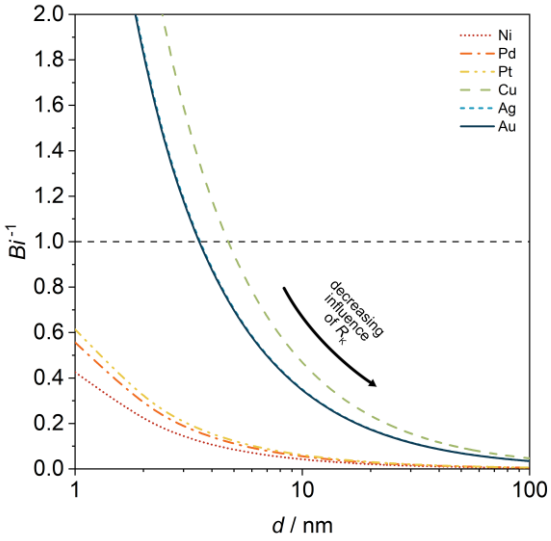

Figure 7. Dependency of the Biot number, in the form of Bi^{-1}, on the particle size, d. The curves are referred to the thermal conductivity of the liquid, κ_L, and the interfacial thermal resistance with each metal, R_K, at T = 298 K.

IV. Conclusions

Density functional theory and non-equilibrium molecular dynamics simulations of a collection of solid-liquid interface models with different transition metals have allowed us to reach the conclusion that the stronger the interactions between species at interfaces, the lower the associated thermal resistance.

The methodology we used here represents a system of practices that lead to interfacial thermal resistance values, R_K, for a wide variety of chemical systems that can be reliably compared with each other. By defining analogous slab-like model architectures and parametrising the potentials for molecular dynamics simulations of their models at the same level of theory, we have overcome the sources of bias that blurred the interpretation of the behaviour of the thermal conductivity of metal-molecular liquids nanofluids in a previous work.[91]

The availability of R_K values enables the use of advanced numerical models for the effective thermal conductivity of nanofluids, which is central for model-based system engineering with

optimisation purposes for the end-use applications such as concentrating solar power, and also the use simple quantities like the Biot number, for prediction and comparison purposes of the expected efficacy of different nanofluids as heat transfer fluids, on the basis of the chemical nature and particle size of the disperse phase. Given the heat-transfer fluid of choice for an application, it is interesting to search for a high thermal conductivity nanomaterial that minimises R_K upon contact with that fluid, and tune the particle size to be as small as possible so that the stability and rheological penalties are minimised, without interface-related detriment to the effective thermal conductivity. Probing the R_K values of solid-liquid interfaces in nanofluids with molecular dynamics facilitates and accelerates the evaluation of thermal conductivity in nanofluids before experimental preparation.

Supplementary Material

Supplementary material includes (i) vibrational frequencies of minimum energy geometries of DPO and BP on Pt surfaces, (ii) input files for MD simulations in LAMMPS and (iii) data for validation of the potentials employed in MD simulations.

Acknowledgments

I.C.-B. acknowledges *Ministerio de Universidades del Gobierno de España* for the allocated budget from the NextGenerationEU programme to public universities for the requalification of the Spanish university system, which funds his postdoctoral position at the University of Cadiz in the form of a *Margarita Salas* fellowship (ref. 2021-067/PN/MS-RECUAL/CD). This work used Young, the UK National Tier 2 High Performance Computing Hub in Materials and Molecular Modelling. We are grateful to the UK Materials and Molecular Modelling Hub for computational resources, which is partially funded by EPSRC (EP/T022213/1, EP/W032260/1 and EP/P020194/1). I.C.-B. thanks Dr. Christopher D. Barret (Mississippi State University, US) for instructions and access to the MEAM Parameter Calibration Tool.

Conflicts of Interest

The authors have no conflicts to disclose.

Author Contributions

I.C.-B.: Conceptualization, Investigation, Formal analysis, Validation, Writing – Original Draft, Visualization, Supervision, Project administration; **J.N.**: Conceptualization, Writing – Review & Editing, Funding acquisition; **R.G.-C.**: Conceptualization, Writing – Review & Editing, Funding acquisition.

Data availability

The data that support the findings of this study are available from the corresponding author upon reasonable request.

References

[1] S. U. S. Choi, and J. A. Eastman, "Enhancing Thermal Conductivity of Fluids with Nanoparticles", *ASME 1995 International Mechanical Engineering Congress & Exposition* (California, USA, Year), **231**, 99-106.

[2] E. Bellos, and C. Tzivadinis, "A review of concentrating solar thermal collectors with and without nanofluids", J. Therm. Anal. Calorim. **135**, 763-786 (2019).

[3] E. A. Chavez Panduro, F. Finotti, G. Largiller, and K. Y. Lervåg, "A review of the use of nanofluids as heat-transfer fluids in parabolic-trough collectors", Appl. Them. Eng. **211**, 118346 1-21 (2022).

[4] IEA, "Technology Roadmap - Concentrating Solar Power" (IEA, Paris, France, 2010).

[5] D. R. Rajendran, E. G. Sundaram, P. Jawahar, S. Sivakumar, O. Mahian, and E. Bellos, "Review on influencing parameters in the performance of concentrated solar power collector based on materials, heat transfer fluids and design", J. Therm. Anal. Calorim. **140**, 33-51 (2019).

[6] M. E. Mondejar, M. Regidor, J. Krafczyk, C. Ihmels, B. Schmid, G. M. Kontogeorgis, and F. Hagling, "An open-access database of the thermophysical properties of nanofluids", J. Mol. Liq. **333**, 115140 1-7 (2021).

[7] G. Tertsinidou, M. J. Assael, and W. A. Wakeham, "The Apparent Thermal Conductivity of Liquids Containing Solid Particles of Nanometer Dimensions: A Critique", Int. J. Thermophys. **36**, 1367-1395 (2015).

[8] K. D. Antoniadis, G. J. Tertsinidou, M. J. Assael, and W. A. Wakeham, "Necessary Conditions for Accurate, Transient Hot-Wire Measurements of the Apparent Thermal Conductivity of Nanofluids are Seldom Satisfied", Int. J. Thermophys. **37**, 78 1-22 (2016).

[9] M. J. Assael, K. D. Antoniadis, W. A. Wakeham, and X. Zhang, "Potential applications of nanofluids for heat transfer", Int. J. Heat Mass Transfer **138**, 597-607 (2019).

[10] P. Keblinski, R. Prasher, and J. Eapen, "Thermal Conductance of Nanofluids: Is the Controversy Over?", J. Nanopart. Res. **10**, 1089–1097 (2008).

[11] Z. Hashin, and S. Shtrikman, "A variational approach to the theory of the effective magnetic permeability of multiphase materials", J. Appl. Phys. **33**, 3125–3131 (1962).

[12] P. Keblinski, S. R. Phillpot, S. U. S. Choi, and J. A. Eastman, "Mechanisms of Heat Flow in Suspension of Nano-sized Particles (Nanofluids)", Int. J. Heat Mass Transfer **45**, 855-863 (2002).

[13] I. Mugica, and S. Poncet, "A Critical Review of the Most Popular Mathematical Models for Nanofluid Thermal Conductivity", J. Nanopart. Res. **22**, 113 1-19 (2020).

[14] D. P. H. Hasselman, "Can the Temperature Dependence of the Heat Transfer Coefficient of the Wire–Nanofluid Interface Explain the “Anomalous” Thermal Conductivity of Nanofluids Measured by the Hot-Wire Method?", Int. J. Thermophys. **39**, 109 1-8 (2018).

[15] M. J. Assael, and W. A. Wakeham, "Comments on “Can the Temperature Dependence of the Heat Transfer Coefficient of the Wire–Nanofluid Interface Explain the “Anomalous” Thermal Conductivity of Nanofluids Measured by the Hot-Wire Method?”", Int. J. Thermophys. **40**, 59 1-15 (2019).

[16] D. P. H. Hasselman, "Response to Comments by M. J. Assael and W. A. Wakeham on: D. P. H. Hasselman, “Can the Temperature Dependence of the Heat Transfer Coefficient of the Wire–Nanofluid Interface Explain the ‘Anomalous’ Thermal Conductivity of Nanofluids Measured by the Hot-Wire Method?”", Int. J. Thermophys. **40**, 60 1-5 (2019).

[17] E. V. Timofeeva, A. N. Gavrilov, J. M. McCloskey, Y. V. Tolmachev, S. Sprunt, L. M. Lopatina, and J. V. Selinger, "Thermal conductivity and particle agglomeration in alumina nanofluids: Experiment and theory", Phys. Rev. E **76**, 061203 1-16 (2007).

[18] L. Xue, P. Keblinski, S. R. Phillpot, S. U.-S. Choi, and J. A. Eastman, "Two Regimes of Thermal Resistance at a Liquid–Solid Interface", J. Chem. Phys. **118**, 337-339 (2003).

[19] L. Xue, P. Keblinski, S. R. Phillpot, S. U.-S. Choi, and J. A. Eastman, "Effect of liquid layering at the liquid–solid interface on thermal transport", Int. J. Heat Mass Transfer **47**, 4277-4284 (2004).

[20] J. Eapen, J. Li, and S. Yip, "Mechanism of Thermal Transport in Dilute Nanocolloids", Phys. Rev. Lett. **98**, 028302 1-4 (2007).

[21] J. Eapen, J. Li, and S. Yip, "Beyond the Maxwell limit: Thermal conduction in nanofluids with percolating fluid structures", Phys. Rev. E **76**, 062501 1-4 (2007).

[22] W. Evans, R. Prasher, J. Fish, P. Meakin, P. Phelan, and P. Keblinski, "Effect of aggregation and interfacial thermal resistance on thermal conductivity of nanocomposites and colloidal nanofluids", Int. J. Heat Mass Transfer **51**, 1431-1438 (2008).

[23] G. Balasubramanian, S. Banerjee, and I. K. Puri, "Unsteady nanoscale thermal transport across a solid-fluid interface", J. Appl. Phys. **104**, 064306 1-4 (2008).

[24] J. M. P. França, C. A. Nieto de Castro, and A. A. H. Pádua, "Molecular interactions and thermal transport in ionic liquids with carbon nanomaterials", Phys. Chem. Chem. Phys. **19**, 17075-17087 (2017).

[25] A. Khodayari, M. Fasano, M. B. Bigdeli, S. Mohammadnejad, E. Chiavazzo, and P. Asinari, "Effect of interfacial thermal resistance and nanolayer on estimates of effective thermal conductivity of nanofluids", Case Studies in Thermal Engineering **12**, 454-461 (2018).

[26] M. R. Hasan, T. Q. Vo, and B. H. Kim, "Manipulating thermal resistance at the solid–fluid interface through monolayer deposition", RSC Adv. **9**, 4948-4956 (2019).

[27] M. Masuduzzaman, and B. H. Kim, "Scale Effects in Nanoscale Heat Transfer for Fourier's Law in a Dissimilar Molecular Interface", ACS Omega **5**, 26527–26536 (2020).

[28] G. Kresse, and J. Hafner, "Ab initio Molecular-Dynamics Simulation of the Liquid-Metal-Amorphous-Semiconductor Transition in Germanium", Phys. Rev. B **47**, 14251-14269 (1994).

[29] G. Kresse, and J. Furthmüller, "Efficiency of Ab-Initio Total Energy Calculations for Metals and Semiconductors Using a Plane-Wave Basis Set", Comput. Mater. Sci. **6**, 15-50 (1996).

[30] G. Kresse, and J. Furthmüller, "Efficient Iterative Schemes for Ab Initio Total-Energy Calculations Using a Plane-Wave Basis Set", Phys. Rev. B **54**, 11169-11186 (1996).

[31] G. Kresse, D. Vogtenhuber, M. Marsman, M. Kaltak, F. Karsai, and M. Schlipf, *Vienna Ab-initio Simulation Package (VASP)*, version 6.3.1 (2022). **https://www.vasp.at**

[32] G. Mills, H. Jónsson, and G. K. Schenter, "Reversible Work Transition State Theory: Application to Dissociative Adsorption of Hydrogen", Surf. Sci. **324**, 305-337 (1995).

[33] H. Jónsson, G. Mills, and K. W. Jacobsen, "Nudged Elastic Band Method for Finding Minimum Energy Paths of Transitions", in *Classical and Quantum Dynamics in Condensed Phase Simulations*, edited by B. J. Berne, G. Ciccotti, and D. F. Coker (World Scientific, 1998), 385-404.

[34] J. P. Perdew, K. Burke, and M. Ernzerhof, "Generalized Gradient Approximation Made Simple", Phys. Rev. Lett. **77**, 3865 3865-3868 (1996).

[35] J. P. Perdew, K. Burke, and M. Ernzerhof, "Erratum: Generalized Gradient Approximation Made Simple", Phys. Rev. Lett. **78**, 1396 1396 (1997).

[36] S. Grimme, J. Antony, S. Ehrlich, and H. Krieg, "A Consistent and Accurate Ab initio Parametrization of Density Functional Dispersion Correction (DFT-D) for the 94 Elements H-Pu", J. Chem. Phys. **132**, 154104 (2010).

[37] S. Grimme, S. Ehrlich, and L. Goerigk, "Effect of the damping function in dispersion corrected density functional theory", J. Comp. Chem. **32**, 1456-1465 (2011).

[38] J. A. Garrido Torres, B. Ramberger, H. A. Früchtl, R. Schaub, and G. Kresse, "Adsorption Energies of Benzene on Close Packed Transition Metal Surfaces Using the Random Phase Approximation", Phys. Rev. Mater. **1**, 060803 1-5 (2017).

[39] G. Kresse, and J. Hafner, "Norm-Conserving and Ultrasoft Pseudopotentials for First-Row and Transition Elements", J. Phys.: Condens. Matter **6**, 8245-8257 (1994).

[40] G. Kresse, and D. Joubert, "From Ultrasoft Pseudopotentials to the Projector Augmented-Wave Method", Phys. Rev. B **59**, 1758-1775 (1999).

[41] H. J. Monkhorst, and J. D. Pack, "Special Points for Brillouin-Zone Integrations", Phys. Rev. B **13**, 5188-5192 (1976).

[42] H. J. Monkhorst, and J. D. Pack, ""Special points for Brillouin-zone integrations" – A Reply", Phys. Rev. B **16**, 1748-1749 (1977).

[43] M. Methfessel, and A. T. Paxton, "High-Precision Sampling for Brillouin-Zone Integration in Metals", Phys. Rev. B **40**, 3616-3621 (1989).

[44] A. Stukowski, "Visualization and analysis of atomistic simulation data with OVITO–the Open Visualization Tool", Modelling Simul. Mater. Sci. Eng. **18**, 015012 (2009).

[45] J. D. Gale, "Empirical Potential Derivation for Ionic Materials", Philos. Mag. B **73**, 3-19 (1996).

[46] J. D. Gale, "GULP: A Computer Program for the Symmetry-adapted Simulation of Solids", J. Chem. Soc., Faraday Trans. **93**, 629-637 (1997).

[47] J. D. Gale, and A. L. Rohl, "The General Utility Lattice Program (GULP)", Mol. Simul. **29**, 291-341 (2003).

[48] J. D. Gale, "GULP: Capabilities and Prospects", Z. Krist. **220**, 552-554 (2005).

[49] J. D. Gale, *General Utility Lattice Program (GULP)*, version 6.1.0 (2022). **http://gulp.curtin.edu.au/gulp/**

[50] S. Plimpton, "Fast Parallel Algorithms for Short-Range Molecular Dynamics", J. Comput. Phys. **117**, 1-19 (1995).

[51] A. P. Thompson, H. M. Aktulga, R. Berger, D. S. Bolintineanu, W. M. Brown, P. S. Crozier, P. J. in't Veld, A. Kohlmeyer, S. G. Moore, T. D. Nguyen, T. Shan, M. J. Stevens, J. Tranchida,

C. Trott, and S. J. Plimpton, "LAMMPS - A Flexible Simulation Tool for Particle-based Materials Modeling at the Atomic, Meso, and Continuum Scales", Comp. Phys.Comm. **271**, 10817 (2022).

[52] S. Plimpton, A. Thompson, S. Moore, A. Kohlmeyer, and R. Berger, *Large Atomic/Molecular Massively Parallel Simulator (LAMMPS)*, version 29Sep2021 (2021). **http://lammps.sandia.gov**

[53] A. I. Jewett, Z. Zhuang, and J.-E. Shea, "Moltemplate a Coarse-Grained Model Assembly Tool", Biophys. J. **104**, 169a (2013).

[54] A. Jewett, *Moltemplate*, version 2.20.4 (2022). **https://www.moltemplate.org**

[55] C. D. Barret, and R. L. Carino, "The MEAM parameter calibration tool: an explicit methodology for hierarchical bridging between ab initio and atomistic scales", Integrating Materials and Manufacturing Innovation **5**, 177-191 (2016).

[56] W. L. Jorgensen, and J. Tirado-Rives, "Potential Energy Functions for Atomic-level Simulations of Water and Organic and Biomolecular Systems", Proc. Natl. Acad. Sci. U.S.A. **102**, 6665-6670 (2005).

[57] L. S. Dodda, J. Z. Vilseck, J. Tirado-Rives, and W. L. Jorgensen, "1.14*CM1A-LBCC: Localized Bond-Charge Corrected CM1A Charges for Condensed-Phase Simulations", J. Phys. Chem. B **121**, 3864-3870 (2017).

[58] L. S. Dodda, I. Cabeza de Vaca, J. Tirado-Rives, and W. L. Jorgensen, "LigParGen Web Server: An Automatic OPLS-AA Parameter Generator for Organic Ligands", Nucleic Acids Res. **45**, 331-336 (2017).

[59] R. W. Hockney, and J. W. Eastwood, "Computer Simulation Using Particles" (Taylor & Francis Group, Abingdon, UK, 1988), 1st edn.

[60] L. Verlet, "Computer "Experiments" on Classical Fluids. I. Thermodynamical Properties of Lennard-Jones Molecules", Phys. Rev. A **159**, 98-103 (1967).

[61] S. Nosé, "A Molecular Dynamics Method for Simulations in the Canonical Ensemble", Mol. Phys. **52**, 255-268 (1984).

[62] S. Nosé, "A Unified Formulation of the Constant Temperature Molecular Dynamics Methods", J. Chem. Phys. **81**, 511-519 (1984).

[63] W. G. Hoover, "Canonical Dynamics: Equilibrium Phase-space Distributions", Phys. Rev. A **1985**, 1695-1697 (1985).

[64] W. G. Hoover, "Constant-Pressure Equations of Motion", Phys. Rev. A **34**, 2499-2500 (1986).

[65] F. Müller-Plathe, "A simple nonequilibrium molecular dynamics method for calculating the thermal conductivity", J. Chem. Phys. **106**, 6082 1-4 (1997).

[66] C. Morin, D. Simon, and P. Sautet, "Chemisorption of Benzene on Pt(111), Pd(111), and Rh(111) Metal Surfaces: A Structural and Vibrational Comparison from First Principles", J. Phys. Chem. B **108**, 5653-5665 (2004).

[67] A. Bilić, J. R. Reimers, N. S. Hush, R. C. Hoft, and M. J. Ford, "Adsorption of Benzene on Copper, Silver, and Gold Surfaces", J. Chem. Theory Comput. **2**, 1093–1105 (2006).

[68] E. Abad, Y. J. Dappe, J. I. Martínez, F. Flores, and J. Orterga, "C6H6/Au(111): Interface dipoles, band alignment, charging energy, and van der Waals interaction", J. Chem. Phys. **134**, 044701 1-8 (2011).

[69] T. S. Chwee, and M. B. Sullivan, "Adsorption studies of C6H6 on Cu (111), Ag (111), and Au (111) within dispersion corrected density functional theory", J. Chem. Phys. **137**, 134703 1-8 (2012).

[70] W. Liu, J. Carrasco, B. Santra, A. Michaelides, M. Scheffler, and A. Tkatchenko, "Benzene Adsorbed on Metals: Concerted Effect of Covalency and van der Waals Bonding", Phys. Rev. B **86**, 245405 1-6 (2012).

[71] W. Liu, V. G. Ruiz, G.-X. Zhang, B. Santra, X. Ren, M. Scheffler, and A. Tkatchenko, "Structure and Energetics of Benzene Adsorbed on Transition-Metal Surfaces: Density-

Functional Theory with van der Waals Interactions Including Collective Substrate Response", New J. Phys. **15**, 053046 1-27 (2013).

[72] H. Yildirim, T. Greber, and A. Kara, "Trends in Adsorption Characteristics of Benzene on Transition Metal Surfaces: Role of Surface Chemistry and van der Waals Interactions", J. Phys. Chem. C **117**, 20572-20583 (2013).

[73] J. Carrasco, W. Liu, A. Michaelides, and A. Tkatchenko, "Insight into the description of van der Waals forces for benzene adsorption on transition metal (111) surfaces", J. Chem. Phys. **140**, 084704 1-10 (2014).

[74] C. Morin, D. Simon, and P. Sautet, "Density-Functional Study of the Adsorption and Vibration Spectra of Benzene Molecules on Pt(111)", J. Phys. Chem. B **107**, 2995–3002 (2003).

[75] S. J. Jenkins, "Aromatic adsorption on metals via first-principles density functional theory", Proc. R. Soc. A **465**, 1-28 (2009).

[76] A. Berg, C. Peter, and K. Johnson, "Evaluation and Optimization of Interface Force Fields for Water on Gold Surfaces", J. Chem. Theory Comput. **13**, 5610–5623 (2017).

[77] J.-P. Jalkanen, and F. Zerbetto, "Interaction Model for the Adsorption of Organic Molecules on the Silver Surface", J. Phys. Chem. B **110**, 5595–5601 (2006).

[78] A. Y. Galashev, K. P. Katin, and M. M. Maslov, "Morse parameters for the interaction of metals with graphene and silicene", Phys. Lett. A **383**, 252-258 (2019).

[79] J. M. Ortiz-Roldan, S. R. G. Balestra, R. Bueno-Perez, S. Calero, E. Garcia-Perez, C. R. A. Catlow, A. R. Ruiz-Salvador, and S. Hamad, "Understanding the stability and structural properties of ordered nanoporous metals towards their rational synthesis", Proc. R. Soc. A **478**, 20220201 1-21 (2022).

[80] B. Lim, M. Jiang, J. Tao, P. H. C. Camargo, Y. Zhu, and Y. Xia, "Shape-Controlled Synthesis of Pd Nanocrystals in Aqueous Solutions", Adv. Funct. Mater. **19**, 189-200 (2009).

[81] S. Alosious, S. K. Kannam, S. P. Sathian, and B. D. Todd, "Kapitza resistance at water–graphene interfaces", J. Chem. Phys. **152**, 224703 1-9 (2020).

[82] S. Alosious, S. K. Kannam, S. P. Sathian, and B. D. Todd, "Nanoconfinement Effects on the Kapitza Resistance at Water–CNT Interfaces", Langmuir **37**, 2355-2361 (2021).

[83] M. R. Azizian, E. Doroodchi, and B. Moghtaderi, in *14th International Heat Transfer Conference*Washington, DC, USA, 2011), pp. 659-665.

[84] M. Milanese, F. Iacobazzi, G. Colangelo, and A. de Risi, "An investigation of layering phenomenon at the liquid–solid interface in Cu and CuO based nanofluids", Int J Heat Mass Trans **103**, 564-571 (2016).

[85] I. Carrillo-Berdugo, R. Grau-Crespo, D. Zorrilla, and J. Navas, "Interfacial molecular layering enhances specific heat of nanofluids: evidence from molecular dynamics", J. Mol. Liq. **325**, 115217 1-8 (2020).

[86] I. Carrillo-Berdugo, S. Midgley, D. Zorrilla, R. Grau-Crespo, and J. Navas, "Understanding the Specific Heat Enhancement in Metal-containing Nanofluids for Thermal Energy Storage: Experimental and Ab-initio evidence for a Strong Interfacial Layering Effect", ACS Appl. Energy Mater. **3**, 9246–9256 (2020).

[87] F. Sofos, T. Karakasidis, and A. Liakopoulos, "Transport properties of liquid argon in krypton nanochannels: Anisotropy and non-homogeneity introduced by the solid walls", Int. J. Heat Mass Transfer **52**, 735-743 (2009).

[88] A. E. Giannakopoulos, F. Sofos, T. Karakasidis, and A. Liakopoulos, "A quasi-continuum multi-scale theory for self-diffusion and fluid ordering in nanochannel flows", Microfluidics and Nanofluidics **17**, 1011–1023 (2014).

[89] D. P. H. Hasselman, and L. F. Johnson, "Effective Thermal Conductivity of Composites with Interfacial Thermal Barrier Resistance", J. Compos. Mater. **21**, 508-515 (1987).

[90] C.-W. Nan, R. Birringer, D. R. Clarke, and H. Gleiter, "Effective thermal conductivity of particulate composites with interfacial thermal resistance", J. Appl. Phys. **81**, 6692-6699 (1997).

[91] I. Carrillo-Berdugo, J. Sampalo-Guzmán, R. Grau-Crespo, D. Zorrilla, and J. Navas, "Interface chemistry effects in nanofluids: experimental and computational study of oil-based nanofluids with gold nanoplates", J. Mol. Liq. **362**, 119762 1-10 (2022).